A radiative transfer model function for 85.5 GHz Special Sensor Microwave Imager ocean brightness temperatures

Thomas Meissner and Frank J. Wentz

Remote Sensing Systems, Santa Rosa, California, USA

Received 6 March 2002; revised 4 June 2002; accepted 18 June 2002; published 5 June 2003.

[1] We analyze vertically and horizontally polarized brightness temperatures at 85.5 GHz that were measured by F15 Special Sensor Microwave Imager (SSM/I) over the world oceans. The columnar liquid cloud water content is restricted to below 0.04 mm. We develop a radiative transfer model function in this frequency region that provides a functional relationship between the measured microwave brightness temperatures and the essential geophysical parameters, which are the atmospheric temperature, ocean surface temperature, and wind speed. This will provide the basis for including the higher SSM/I, Tropical Rainfall Measurement Mission Microwave Imager (TMI), and Advanced Microwave Scanning Radiometer frequency channels into oceanic and atmospheric retrieval algorithms, which rely on an accurate forward model. *INDEX TERMS:* 6969 Radio Science: Remote sensing; 6959 Radio Science: Radio oceanography; 6904 Radio Science: Atmospheric propagation; *KEYWORDS:* radiative transfer model, SSM/I, 85.5 GHz

Citation: Meissner, T., and F. J. Wentz, A radiative transfer model function for 85.5 GHz Special Sensor Microwave Imager ocean brightness temperatures, *Radio Sci., 38*(4), 8066, doi:10.1029/2002RS002655, 2003.

1. Introduction

[2] Because of the lack of an accurate, consistent geophysical model function for the measured brightness temperatures of the high-frequency channels of airborne passive microwave sensors (85.5 GHz at Special Sensor Microwave Imager (SSM/I) and Tropical Rainfall Measurement Mission Microwave Imager (TMI) and 89 GHz at Advanced Microwave Scanning Radiometer (AMSR)), these channels have so far not been included into the Remote Sensing Systems well-calibrated retrieval algorithms [*Wentz*, 1997], which rely on an accurate geophysical forward model. The 85.5 GHz SSM/I has been used in data assimilation systems for numerical weather predictions [*Phalippou*, 1996; *Prigent et al*., 1997], which adopt a variational approach and are therefore able to tolerate larger forward model errors at 85.5 GHz without completely dropping the channel.

[3] In the absence of rain the brightness temperature T_B that is received by the satellite depends on the following: (1) the sea surface temperature (SST), T_S, (2) the atmospheric temperature profile, $T(z)$, (3) the atmospheric air pressure profile, $p(z)$, (4) the atmospheric profile of water vapor density, $\rho_V(z)$, (5) the atmospheric profile of liquid cloud water density, $\rho_L(z)$, (6) the ocean surface wind speed, W, and (7) the ocean surface wind direction (relative to the looking azimuth), φ. It is the aim of our study to derive a model function depending on these geophysical parameters for vertical (v) and horizontal (h) polarization and Earth incidence angles of $\sim$53° from 85.5 GHz SSM/I observations.

[4] The 85.5 GHz channel is very sensitive to cloud absorption. In order to not swamp the signals for vapor, SST, and wind, we consider only cases with low columnar cloud liquid water content, i.e., $L \leq 0.04$ mm. Furthermore, we will consider only the isotropic wind response of the ocean surface for the moment and neglect the dependence on wind direction.

2. Study Data Set

[5] For our analysis we are using brightness temperatures that were measured by F15 SSM/I during 2002. SSM/I also provides values for the columnar water vapor

$$V = \int_0^H dz\ \rho_V(z),$$

the columnar liquid cloud water

$$L = \int_0^H dz\ \rho_L(z),$$

and the surface wind speed W. H denotes the satellite altitude. All observations are binned into 0.25° latitude (LAT)-longitude (LON) maps. Because of the restriction $L \leq 0.04$ mm, they are automatically filtered for

0048-6604/03/2002RS002655$11.00

rain. V, L, and W are retrieved using only the 19, 22, and 37 GHz channels of the SSM/I instrument [*Wentz*, 1997].

[6] The atmospheric profiles of $T(z)$, $p(z)$, $\rho_V(z)$, and $\rho_L(z)$ as well as the SST T_S are obtained from the National Centers for Environmental Prediction (NCEP) final analysis, which is available four times daily on a 1° LAT-LON grid. The NCEP events are trilinearly interpolated to the SSM/I events in LAT, LON, and time. The numerical weather prediction moisture analyses are accurate to 10% at best. We therefore scale the NCEP water vapor density $\rho_V(z)$ so that its columnar integral equals the SSM/I value.

3. Radiative Transfer Equation

[7] In general, the brightness temperature that is received by the satellite is given by the following radiative transfer equation:

$$T_B = T_{BU} + \tau E T_S + \tau (1 - E)\, T_{BD}(1 + \Omega_{\text{scat}}) + \tau^2(1 - E)T_C, \tag{1}$$

where E is the sea surface emissivity and depends on T_S, W, and φ. The total atmospheric transmittance is denoted by τ and is given by

$$\tau = \exp[-\sec(\theta)(A_O + A_V + A_L)], \tag{2}$$

where the A_I is the columnar integral over the atmospheric absorption coefficients α_1 for $I = O$ (oxygen), V (water vapor), and L (liquid cloud water) as follows:

$$A_I = \int_0^H dz\ \alpha_I(z). \tag{3}$$

[8] T_{BU} is the upwelling atmospheric brightness temperature, and T_{BD} is the downwelling atmospheric brightness temperature that is reflected at the sea surface. Both quantities are given as weighted integrals of the atmospheric temperature profiles

$$T_{BU} = \sec(\theta) \int_0^H dz\ \sum_I \alpha_I(z)\ T(z)\ \tau(z,H,\theta)$$

$$T_{BD} = \sec(\theta) \int_0^H dz\ \sum_I \alpha_I(z)\ T(z)\ \tau(0,z,\theta) \tag{4}$$

where

$$\tau(h_1,h_2,\theta) \equiv \exp\left[-\sec(\theta) \int_{h_1}^{h_2} dz \sum_I \alpha_I(z) \right]$$

and $\tau = \tau(0,H,\theta)$. The scatter term Ω_{scat} correction accounts for the fact that, for a wind-roughened sea surface, radiation can be reflected from directions of the sky other than the specular direction. $T_C = 2.7$ K is the cold space radiation.

4. Dielectric Constant of Seawater

[9] A major input into the radiative transfer model is the dielectric constant of seawater ε. It determines the specular sea surface emissivity E_0 for both v and h polarization on the basis of the Fresnel equations

$$E_{0v} = 1 - \left| \frac{\varepsilon \cos(\theta) - \sqrt{\varepsilon\text{-}\sin^2(\theta)}}{\varepsilon \cos(\theta) + \sqrt{\varepsilon\text{-}\sin^2(\theta)}} \right|^2$$

$$E_{0h} = 1 - \left| \frac{\cos(\theta) - \sqrt{\varepsilon\text{-}\sin^2(\theta)}}{\cos(\theta) + \sqrt{\varepsilon\text{-}\sin^2(\theta)}} \right|^2. \tag{5}$$

[10] *Guillou et al.* [1998] have recently provided laboratory measurements of this quantity at 85.5 and 89 GHz. Alternatively, one can predict ε for a frequency ν from the Debye dipole relaxation theory [*Debye*, 1929]

$$\varepsilon(\nu) = \varepsilon_\infty + \frac{\varepsilon_0 - \varepsilon_\infty}{1 + [i\nu/\nu_R]^{1-\eta}} - \frac{2i\sigma}{\nu}. \tag{6}$$

[11] The value ε_0 denotes the value for the static dielectric constant, ε_∞ denotes its value at infinite frequency, σ denotes the seawater conductivity, η denotes the Cole-Cole spread factor [*Cole and Cole*, 1941], ν_R denotes the Debye relaxation frequency, and $i=\sqrt{-1}$. The values ε_∞, ε_0, σ, and ν_R depend on SST. In addition, ε_0, σ, and ν_R depend on the salinity of seawater. The value η is an empirical constant, which describes the spread of the relaxation wavelengths. A model for these parameters was provided by *Wentz and Meissner* [1999] which updates an earlier work by *Klein and Swift* [1977]. The analysis is based on measurements at low frequencies and has proven to describe well the frequency dependence of ε for frequencies below 37 GHz. At 85.5 GHz, both methods are consistent in warm water $T_S > 20$°C, whereas in cold water there are substantial differences. For example, the specular surface emissions $E_0 T_S$ for both v and h polarization are ~3.5 K lower in the case of *Guillou et al.* [1998] than in case of the Debye model. A more elaborate Debye model containing two different relaxation wavelengths has been developed by *Liebe et al.* [1991] for fresh water and by *Stogryn et al.* [1995] for freshwater and seawater. Recent airborne measurements by the Millimeter-Wave Imaging Radiometer at 89 GHz [*Wang*, 2002] favor the model of *Stogryn et al.* [1995]. It is one aim of our study to provide a validation for ε at 85.5 GHz from SSM/I measurements.

5. Atmospheric Absorption

[12] The atmospheric absorption models relate the absorption coefficients α_1, $I = O$, V, and L to the

atmospheric profiles for temperature, pressure, water vapor, and liquid cloud water.

5.1. Oxygen Absorption

[13] We use the oxygen absorption coefficients provided by P. W. Rosenkranz (personal communication, 1998). These coefficients are based on the work by *Liebe et al*. [1992] and *Schwartz* [1997].

5.2. Water Vapor Absorption

[14] The 85.5 GHz channel lies in the water vapor window and is therefore very sensitive to the water vapor continuum absorption. An updated and comprehensive analysis has been performed by *Rosenkranz* [1998], who uses a combination of the millimeter wave propagation models (MPM) created by *Liebe and Layton* [1987] (MPM 87) for the foreign-broadened continuum and by *Liebe et al*. [1993] (MPM 93) for the self-broadened continuum. This combination has been validated against numerous experimental observations [*Westwater et al*., 1990]. An exception is found in upward looking combined aircraft-radiosonde measurements by *English et al*. [1994]. In a moist atmosphere (V = 45 mm) their measurements show a larger absorption than the model of *Rosenkranz* [1998].

[15] Very recently, an atmospheric radiative transfer model, called MonoRTM, has been developed by Atmospheric and Environmental Research, Inc. (AER) [*Boukabara et al*., 2002]. It is the aim of this paper to compare the two water vapor models by *Rosenkranz* [1998] and *Boukabara et al*. [2002] using the SSM/I data.

5.3. Liquid Cloud Water Absorption

[16] For the liquid cloud water absorption, we use the Rayleigh approximation

$$\alpha_L = \frac{6\ \pi\ \rho_L}{\lambda}\ \mathrm{Im}\left(\frac{1-\varepsilon}{2+\varepsilon}\right), \tag{7}$$

where λ is the radiation wavelength (in cm), ρ_L is the liquid cloud water density (in units of g/cm^3), and ε is the dielectric constant of cloud (pure) water. For ε at 85.5 GHz we have used the model of *Liebe et al*. [1991]. The liquid cloud water absorption for the low liquid cloud water content $L \leq 0.04$ mm is rather insensitive to ε even if supercooled clouds are included. We have found no noticeable difference when using the dielectric model of *Stogryn et al*. [1995].

6. Special Sensor Microwave Imager (SSM/I) Analysis for Specular Sea Surface

[17] For low wind speeds $W \leq 5$ m/s the 85.5 GHz v polarization brightness temperature changes very little with wind speed and is therefore independent on the sea surface roughness. This provides a convenient way to measure the properties of the specular emission and the atmospheric transmittance at this frequency.

6.1. Validation of the Dielectric Properties of Seawater

[18] In order to analyze the temperature dependence of the dielectric constant of seawater we need to avoid possible errors that can arise owing to deficiencies of the water vapor absorption model because of the strong geographic correlation between SST and water vapor. We first confine ourselves to dry atmospheres where the total vapor content is <15 mm. Figure 1 shows the difference $T_B - F$ between the measured brightness temperatures T_B and the computed model function F. We have used the values of the dielectric constant from *Guillou et al*. [1998] (model 1; top panel of Figure 1), the prediction by the Debye theory with the parameters of *Wentz and Meissner* [1999] (model 2; middle panel of Figure 1), and the double Debye relaxation model of *Stogryn et al*. [1995] (model 3; bottom panel of Figure 1). The results are binned with respect to SST in the interval between 0° and 25°C. The bin population is ~30,000 events for the lowest SST bin and is decreasing to ~1200 events in the highest SST bin. In computing the model function F we have used the water vapor absorption model of *Rosenkranz* [1998]. As we will show in the next section, the difference to the MonoRTM [*Boukabara et al*., 2002] is very small in dry atmospheres.

[19] For all three models in Figure 1 we observe small overall biases (−1.3 K for model 1, −2.1 K for model 2, and −2.2 K for model 3). These brightness temperature offsets arise because of deficiencies in the dielectric constant model itself, instrument calibration errors, and deficiencies in the atmospheric absorption model, especially the oxygen absorption, which is nearly constant over the world oceans. At this point it is not possible to separate these effects. In order to assess which of the three models fits the data best, we need to look at the average quadratic deviation of each bin from a constant line, which is given by the overall biases mentioned above. Quantitatively, this is given by the expression $\sqrt{\chi^2/(n-1)}$. The total number of bins is denoted by n, which is 13 in this case, and $\chi^2 = \sum_{i=1}^{n} w_i (y_i - \bar{y})^2$, where y_i is the average of $T_B - F$ in each bin, $\bar{y}$ is the overall bias of $T_B - F$ and the w_i are appropriate weights for each bin. We use $w_i = 1$. The results are 0.48 K (model 1), 1.45 K (model 2) and 0.83 K (model 3). Furthermore, we observe that for model 1 the deviations from the overall bias are basically constant over the whole SST range. For model 2, $T_B - F$ increases monotonically by ~3.0 K over the SST range. For model

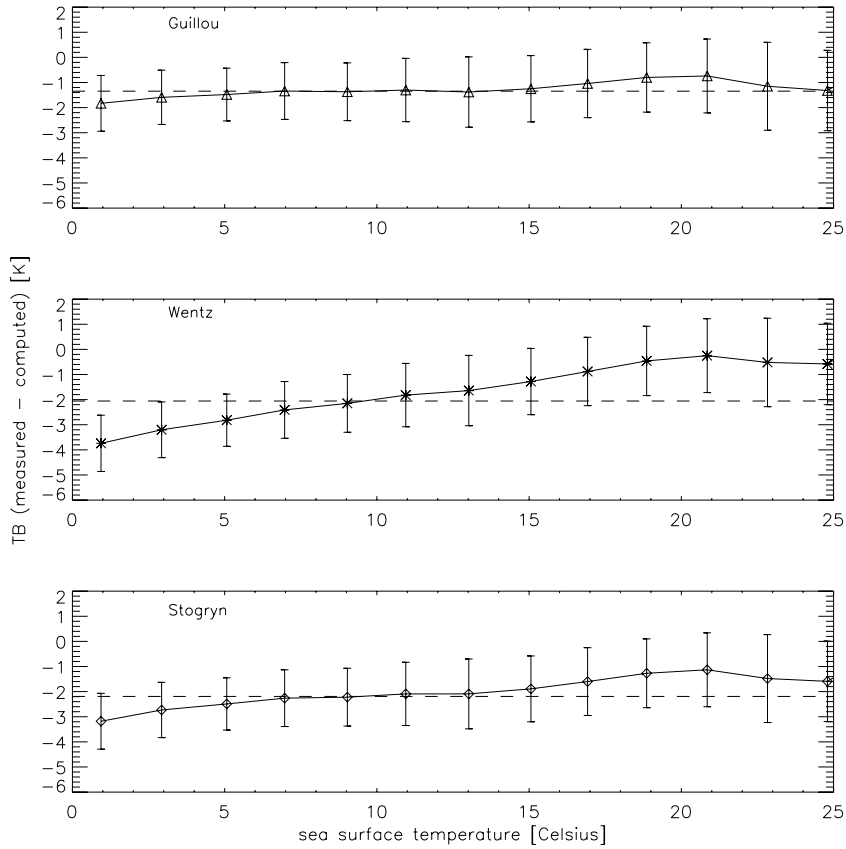

Figure 1. Difference between the measured Special Sensor Microwave Imager (SSM/I) 85.5 GHz *v* polarization brightness temperatures and the geophysical model function for sea surface temperatures (SST) between 0° and 25°C using a dry atmosphere with a columnar water vapor <15 mm and a specular sea surface. The top panel shows the results for a dielectric constant of seawater measured by *Guillou et al*. [1998], the middle panel shows the results for the model of *Wentz and Meissner* [1999], and the lower panel shows the results for the model of *Stogryn et al*. [1995]. The size of the SST bins is 2 K. The overall T_B biases are −1.3 K, −2.1 K, and −2.2 K, respectively, and are indicated with dashed lines.

3 the increase is much less, ~1.5 K. These values are to be compared with the values of the error bars σ in each bin, which are between 1.1 and 1.7 K. This supports the measurements of *Guillou et al*. [1998] for dielectric constant of seawater at 85.5 GHz. It also shows that the double Debye relaxation model fits the data noticeably better than the single Debye relaxation model.

6.2. Validation of the Water Vapor Absorption Models

[20] Having validated the measurement for the dielectric constant of seawater of *Guillou et al*. [1998], we will use their value from now on and extend the analysis to the whole water vapor region between 2 and 60 mm and test the vapor absorption models by *Rosenkranz* [1998] and the AER MonoRTM [*Boukabara et al*., 2002]. The bin size is 2 mm. The population of the lowest vapor bin is ~500 events, increasing to just above 60,000 events for vapor bins above 15 mm. Figure 2 displays the difference between measured and computed brightness temperatures. In the upper panel of Figure 2 we have used the columnar water vapor V from SSM/I and, as mentioned earlier, scaled the NCEP profiles so that their value of total vapor content agrees with the SSM/I value. Both models in Figure 2 give very similar results: There are basically no differences for $V < 10$ mm. For moist atmospheres ($V > 40$ mm) the MonoRTM gives a smaller absorption amounting to a computed brightness temperature that is smaller than the *Rosenkranz* [1998] model gives. The values for the overall biases are +0.4 K

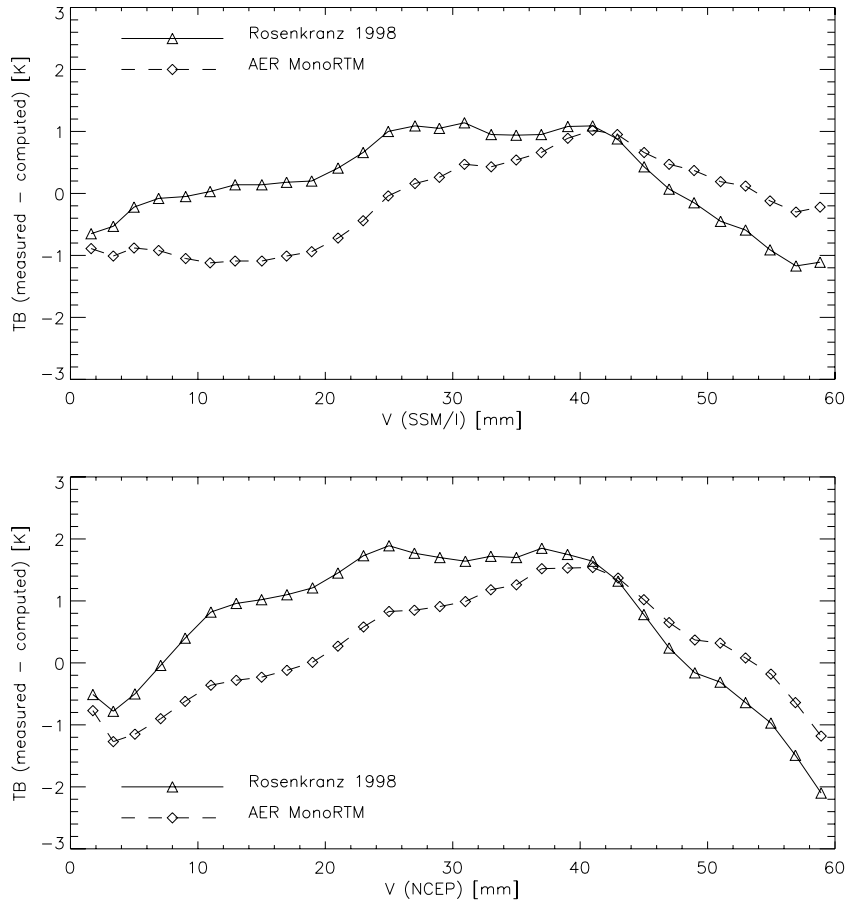

Figure 2. Difference between the measured SSM/I 85.5 GHz *v* polarization brightness temperatures for a specular sea surface and the geophysical model function for columnar water vapor values between 2 and 50 mm. The size of the water vapor bins is 2 mm. The dielectric constant of seawater is taken from *Guillou et al*. [1998]. The triangles and solid lines correspond to the atmospheric absorption model of *Rosenkranz* [1998], whereas the diamonds and dashed lines correspond to the Atmospheric and Environmental Research, Inc. MonoRTM [*Boukabara et al*., 2002]. For the top panel the National Centers for Environmental Prediction (NCEP) water vapor profiles have been scaled so that the total columnar water vapor equals the SSM/I value. For the bottom panel we have used the unscaled NCEP water vapor profiles.

(for the *Rosenkranz* [1998] model) and −0.2 K (for the MonoRTM). The values for $\sqrt{\frac{\chi^2}{n-1}}$ are 0.75 K and 0.73 K, respectively, and are to be compared with typical values of 3.3 K for the error bars in each vapor bin. This means that the MonoRTM vapor model fits the data slightly better than the *Rosenkranz* [1998] model. We cannot see the observed deficiency of the model absorption reported by *Rosenkranz* [1998] when comparing his model with the measurements by *English et al*. [1994] (compare section 5.2).

[21] For comparison, the bottom panel of Figure 2 shows the results if the NCEP profiles are not scaled and the columnar water vapor from NCEP instead of the SSM/I value is used. The fluctuations of $T_B - F$ around the mean increase. Therefore the values for $\sqrt{\frac{\chi^2}{n-1}}$ also increase to 1.21 and 0.90, respectively, but the basic pattern and conclusions remain the same.

7. SSM/I Analysis of the Isotropic Wind-Induced Emissivity

[22] The emissivity of the wind-roughened ocean surface differs from the specular emissivity owing to the following:

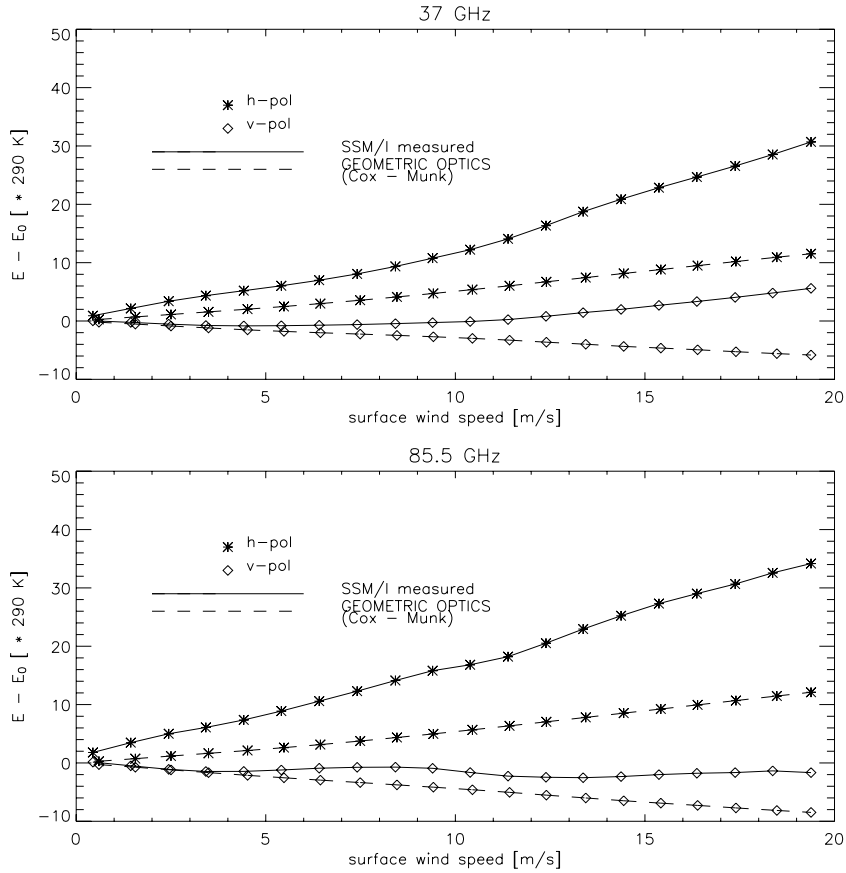

Figure 3. Wind-induced sea surface emissivity (measured-specular emissivity) for the SSM/I (top) 37 GHz and (bottom) 85.5 GHz channels. The results for the *v* polarization are indicated by diamond symbols and for the *h* polarization by star symbols. The wind speeds were measured by QuikScat and refer to 10 m above ground. The size of the wind speed bins is 1 m/s. The solid lines denote the SSM/I measurements. The dashed lines denote the results of the Geometric Optics model as specified by *Wentz and Meissner* [1999] using the Cox-Munk slope distribution [*Cox and Munk*, 1954].

1. The presence of large gravity waves. This is commonly treated in the Geometric Optics (GO) model (Kirchhoff Approximation) using an ensemble of tilted facets, each acting as a specular tilted surface [*Stogryn*, 1967]. The slope variance of the tilted facets increases proportionally with wind speed [*Cox and Munk*, 1954].

2. The presence of small capillary waves resulting in Bragg Scattering.

3. The appearance of sea foam at larger wind speeds $W \geq 7$ m/s.

[23] For the lower-frequency channels, it has turned out that a satisfactory theoretical modeling of all these effects is very difficult [*Wentz and Meissner*, 1999; *Wentz*, 1997]. We do not attempt to do this but derive the wind induced isotropic sea surface emissivity $\Delta E(W,T_S) = E - E_0$ empirically from SSM/I observations. The only exception is the scatter term Ω_{scat} in equation (1), which has to be removed from the measured T_B in order to extract the sea surface emissivity. We calculate this term using the GO model [*Wentz and Meissner*, 1999; *Wentz*, 1997] at 85.5 GHz.

[24] Figure 3 shows the results for the wind-induced emissivities at 85.5 and 37 GHz, binned with respect to wind speed between 0 and 20 m/s. The bin size is 1 m/s. The bin population ranges from ~3000 at 20 m/s to over 300,000 at 7 m/s. For the computation we have used the dielectric constant of [*Guillou et al*., 1998] and the water vapor absorption model of MonoRTM, both of which we validated in section 6. The range of the water vapor comprises the interval between 2 and 40 mm. For comparison, we have also included the results of the GO model with the Cox-Munk slope distribution [*Cox and*

Munk, 1954] as specified by *Wentz and Meissner* [1999]. We note that the 85.5 GHz *v* polarization wind speed signal is basically zero over the whole wind speed range. For a surface wind speed of 15 m/s the *h* polarization wind speed signal increases by ~25% from 37 to 85.5 GHz. A similar observation was made by *Rosenkranz* [1992].

[25] Interesting also is the deviation between the observed emissivities and the GO model, which is noticeably larger at 85.5 GHz than at 37 GHz. At higher wind speeds this is likely due to the larger emissivity of sea foam at the higher frequency. At low wind speeds the observed difference can arise from the presence of capillary waves, as mentioned above, or it could point to an insufficiency of the Cox-Munk slope distribution, which has been used in the GO calculation.

8. Summary and Conclusions

[26] Our study of the 85.5 GHz SSM/I *v* and *h* polarization channels for low cloud cases validates the measurements for the dielectric of seawater by *Guillou et al*. [1998] and the water vapor continuum absorption models by *Rosenkranz* [1998] and the AER MonoRTM [*Boukabara et al*., 2002]. We also provide a prediction for the isotropic wind-induced sea surface emissivity.

[27] In order to complete this analysis, we will include cases for larger liquid cloud water and study the liquid cloud water absorption at 85.5 GHz in more detail. We also plan to investigate the size of the wind direction signal at this frequency.

[28] **Acknowledgments.** This research was funded by NASA contract NAS5-32594 (AMSR). We are thankful to P. W. Rosenkranz for the FORTRAN codes for calculating the water vapor and oxygen absorption coefficients, to S. Boukabara (AER) for the FORTRAN code of the MonoRTM, and to P. Wang for the FORTRAN codes for the double Debye model of *Stogryn et al*. [1995].

References

Boukabara, S. A., S. A. Clough, and R. N. Hoffman, MonoRTM: A monochromatic radiative transfer model for microwave and laser calculations, Atmos. and Environ. Res., Lexington, Mass., 2002.

Cole, K. S., and R. H. Cole, Dispersion and absorption in dielectrics, *J. Chem. Phys.*, *9*, 341–351, 1941.

Cox, C. S., and W. H. Munk, Measurement of the roughness of the sea surface from photographs of the Sun's glitter, *J. Opt. Soc. Am.*, *44*, 838–850, 1954.

Debye, P., *Polar Molecules*, Dover, Mineola, N. Y., 1929.

English, S. J., C. Guillou, C. Prigent, and D. C. Jones, Aircraft measurements of water vapour continuum absorption at millimetre wavelength, *O. J. R. Meteorlol. Soc.*, *120*, 603–625, 1994.

Guillou, C., W. Ellison, L. Eymard, K. Lamkaouchi, C. Prigent, G. Delbos, G. Balana, and S. A. Boukabara, Impact of new permittivity measurements on sea surface emissivity modeling in microwaves, *Radio Sci.*, *33*(3), 649–667, 1998.

Klein, L. A., and C. T. Swift, An improved model for the dielectric constant of sea water at microwave frequencies, *IEEE J. Oceanic Eng.*, *2*, 104–111, 1977.

Liebe, H. J., and D. H. Layton, Millimeter-wave properties of the atmosphere: Laboratory studies and propagation modeling, Natl. Telecommun. and Inf. Admin., Boulder, Colo., 1987.

Liebe, H. J., G. A. Hufford, and T. Manabe, A model for the complex permittivity of water at frequencies below 1 THz, *Int. J. Infrared Millimeter Waves*, *12*(7), 659–675, 1991.

Liebe, H. J., P. W. Rosenkranz, and G. A. Hufford, Atmospheric 60-GHz oxygen spectrum: New laboratory measurements and line parameters, *J. Quant. Spectrosc. Radiat. Transfer*, *48*, 629–643, 1992.

Liebe, H. J., G. A. Hufford, and M. G. Cotton, Propagation modeling of moist air and suspended water/ice particles at frequencies below 1000 GHz, *AGARD Conf. Proc.*, *12*, 3.1–3.10, 1993.

Phalippou, L., Variational retrieval of humidity profile, wind speed and cloud-liquid water path with the SSM/I: Potential for numerical weather prediction, *Q. J. R. Meteorol. Soc.*, *122*(530), 327–355, 1996.

Prigent, C., L. Phalippou, and S. English, Variational inversion of the SSM/I observations during the ASTEX campaign, *J. Appl. Meteorol.*, *36*, 493–508, 1997.

Rosenkranz, P. W., Rough-Sea Microwave Emissivities Measured with the SSM/I, *IEEE Trans. Geosci. Remote Sens.*, *30*(5), 1081–1085, 1992.

Rosenkranz, P. W., Water vapor microwave continuum absorption: A comparison of measurements and models, *Radio Sci.*, *33*(4), 919–928, 1998.

Schwartz, M.J., Ph.D. thesis, Massachusetts Inst. of Technol., Cambridge, Mass., 1997.

Stogryn, A., The apparent temperature of the sea at microwave frequencies, *IEEE Trans. Antennas Propag.*, *AP-15*, 278–286, 1967.

Stogryn, P. A., H. T. Bull, K. Rubayi, and S. Iravanchy, The microwave permittivity of sea and fresh water, GenCorp Aerojet, Azusa, Calif., 1995.

Wang, J. R., A comparison of the MIR-estimated and model-calculated fresh water surface emissivities at 89, 150 and 220 GHz, *IEEE Trans. Geosci. Remote Sens*, *40*(6), 1356–1365, 2002.

Wentz, F., and T. Meissner, AMSR ocean algorithm, version 2, Remote Sensing Systems, Santa Rosa, Calif., 1999.

Wentz, F. J., A well-calibrated ocean algorithm for special sensor microwave/imager, *J. Geophys. Res.*, *102*(C4), 8703–8718, 1997.

Westwater, E.R., J.B. Snider, and M.J. Falls, Ground-based radiometric observations of atmospheric emission and attenuation at 20.6, 31.65 and 90.0 GHz: A comparison of measurement and theory, *IEEE Trans. Antennas Propag.*, *38*, 1569–1580, 1990.

T. Meissner and F. J. Wentz, Remote Sensing Systems, 438 First Street, Suite 200, Santa Rosa, CA 95401, USA. (meissner @remss.com; wentz@remss.com)